Miniaturized Optimal Incident Light Angle-fitted Dark Field System for Contrast-enhanced Real-time Monitoring of 2D/3D-projected Cell Motions

Yeongseok Jang
Jeonbuk National University
Seungbeom Han
Jeonbuk National University
Chulgyu Song
Jeonbuk National University
Jinmu Jung
Jeonbuk National University
Jonghyun Oh (jonghyuno@jbnu.ac.kr)
Jeonbuk National University

Research Article

Keywords: Miniaturized Optimal, subcellular structures, nanotubes

Posted Date: December 30th, 2021

DOI: https://doi.org/10.21203/rs.3.rs-1194147/v1

Abstract

In the field of biology, dark field microscopy provides superior insight into cells and subcellular structures. However, most dark field microscopes are equipped with a dark field filter and a light source on a 2D-based specimen, so only a flat sample can be observed in a limited space. We propose a compact cell monitoring system with built-in dark field filter with an optimized incident angle of the light source to provide real-time cell imaging and spatial cell monitoring. 2D/3D projected darkfield images are optimized for 2D/3D samples as they rely on darkfield filters, and incident light. 2D projection imaging was implemented using a modular condenser lens to acquire high-contrast images. This enabled the long-term monitoring of cells, and the real-time monitoring of cell division and death. This system was able to image, by 2D projection, cells on the surface thinly coated with multi-walled carbon nanotubes, as well as living cells that migrated along the surface of glass beads and hydrogel droplets with a diameter of about 160 μm. The Optimal incident light angle-fitted dark field system combines high-contrast imaging sensitivity and high spatial resolution to even image cells on three-dimensional surfaces.

Introduction

Cellular activities have been proven to exert a powerful effect on cellular morphology and viability. The importance of live cell visualization and monitoring is that can provide a predictive insight as to how the cells interact and process in the fields of biomedical applications. Researchers have been challenged to achieve a more spatially detailed visualization and monitoring of single- or multiple-cell observation on three-dimensional structures. These engineering challenges have introduced advances in diverse live-cell imaging systems.

Recent advances in live cell imaging have been developed with confocal, light-sheet, holographic, or multi-photon microscopies. These can provide super-resolution of 3D volumetric images of cellular structures up to nanoscales, as well as reduce phototoxicity. To enhance the 3D spatial resolution, these require multiple optical sectioning and reconstructing processes, which are limited in both the taking of images in broad dynamic cell ranges, and the monitoring of long-term cell activities [1-3].

In situ direct microscopic imaging and monitoring of cell activities has attracted considerable attention in comprehensive approaches using luminescence. Conventionally, the refractive index (RI) has played an important role in the enhanced visualization of transparent living cells using phase contrast microscopy or differential interference microscopy, which could enhance contrast due to optical interferometry [4-7]. Optical diffraction tomography (ODT), the quantitative refractive index imaging technique, was developed to provide three-dimensional cell structures [8-12]. However, the disadvantage is that the projected two-dimensional images can be distorted due to internal diffraction and refraction of the object, which limits the monitoring of lively moving cells in both the short- and long-term [13]. In addition, the conventional bright field illumination-based tools have been limited in closely observing the behavior of transparent specimen, like cells and organisms, without additional cell treatment [14-20].

One of the luminescence-based systems that can closely observe transparent specimen like cells and organisms is dark field microscopy. Optical discontinuities from cell membrane, lipid, nucleus, and internal organelles enable dark field illumination to visualize these cell parts clearly on a black background [21]. The images produced by dark field microscopy show improved sharpness and contrast-enhanced 3D volume of cells because of a physical filter. Wei et al. developed a new *in situ* dark field probe consisting of an aspheric condenser and relay lens that improved the sharpness of the images for on-line monitoring of yeast cell density and viability [22]. Taylor et al. showed enhanced sensitivity in dark field microscopy by optimizing the illumination angle to suppress the background of unwanted scattered light [23]. Cybulski et al. introduced a low-cost, portable origami-based paper microscope demonstrating brightfield, darkfield, and fluorescence microscopes in science and education [24]. Walzik et al. described a low-cost, portable live-cell imaging system with bright and dark field for time-resolved label-free visualization of dynamic processes in living cells [25]. Sharkey et al. fabricated a one-piece 3D printed flexure translation stage for open-source microscopy that could allow the samples to be held stably in the focal plane, and translated to features of interest [26]. Jung et al. presented a portable multi-contrast microscope capable of producing bright field, dark field, and different phase contrast images of thin biological specimens on a smartphone platform [27]. Sun et al. introduced a low-cost mobile phone dark field microscope for nanoparticle-based quantitative studies in biomedical applications [28]. Huang et al. provided a laser and dark field microscopic platform for long-term studies of the relationship between plasmonic NPs and changes in the morphology of specifically positioned cells *in vitro* [29]. Guo et al. used dark field microscopy based on localized surface plasmon resonance for HER2 protein imaging on cell surfaces [30].

In this study, we demonstrate a new low-cost (less than $360), portable dark field microscopic cell imaging and monitoring system. The optimal angle of light incident on transparent cells in the system could serve high-contrast cell imaging and monitoring obtained by 3D projection onto a 2D plane for short- and long-term in the incubator. The system consisted of a newly developed illumination module (including LED light, dark field filter, and condenser lens), and camera module (including CMOS sensor with reversed camera lens and body tube). The dark field filter (DFF) in the system was designed focusing on an optimal incident light angle that could suppress light scattering of the dark background, resulting in the enhanced 3D projection onto a 2D plane. Its contrast-enhanced high resolution could make definite on-line monitoring functions of cell density and viability on 2D and 3D cell culture environments, which was feasible for *in situ* imaging and analysis in the incubator.

Materials And Methods

Dark field cell monitoring system (DFCMS) design

Figure 1a shows a schematic and prototype of the designed cell monitoring system (CMS). The main structure of the system was designed by 3D modeling program (Catia V5R18, Dassault Systems, Concord, MA, USA), and then drawn by AutoCAD (Autodesk Inc., San Francisco, CA, USA). The system

was fabricated through aluminum processing. Its fixed size was 12 cm (width) x 12 cm (depth) x 18 cm (height). It was designed in a manner similar to an Inverted microscope to mount cell culture plates, cell culture dishes, and other paraphernalia. In addition, XYZ-axis precision stages (LD40-LM XYZ40-LM, ZY automation store, Shanghai, China) were installed to easily adjust the focus of the specimens.

Configuration and optimization of the compact optical module

The fabricated compact optical module was composed of a CMOS (IMX214 1/3.06 inch, Sony, Minato, Tokyo, Japan) imaging module and the plastic lens of a commercial camera (ELP 13 Megapixel USB Webcam, Ailipu Technology Co., Ltd., Shenzhen, Guangdong, China) with a resolution of 13 MP. The imaging module could be powered by USB with an operating voltage of 5 V DC, and transmitted data simultaneously. After disassembling the lens from the imaging module, it was inverted in the reverse direction. The objective lens was combined with a barrel made with a 3D printer (Form2, FormLabs Inc., Somerville, MA, USA). Unlike conventional commercial cameras, this compact optical module was used to enlarge objects using a reverse macro method. To achieve the target magnification of the compact optical module, the body tube length was experimentally determined to be 18 mm from the CMOS sensor to the lens. A white LED (1 W) was used for the light source of the illumination part. The drive voltage and current of the LED were 3 V and 320 mA, respectively. They were powered through the external port of the camera module.

An aspherical lens having a focal length of 30 mm (Plano-Convex Lens; 48656, Edmund Optics, Barrington, NJ, USA) was used as a condenser lens for collecting light. The dark field filter (DFF) to be combined with the condenser lens was designed using a 3D modeling program (Catia V5R18, Dassault Systems, Concord, MA, USA), and printed using a 3D printer. The black color resin (Black V4, Formlabs Inc., Somerville, MA, USA) was chosen as the material for the dark field patch, because it reduces gloss and minimizes diffuse reflection. For high contrast of dark field imaging, dark field filters (DFF_{ID}) with five kinds of inside diameter were designed, fabricated, and tested with light-blocking center diameters of (19, 20, 21, 22, and 23) mm, respectively, as shown in Fig. 1b. Figure 1c shows that the cell monitoring system could resolve square lines as closely spaced as 2.76 μm with dark peak separation. Such high resolution is enough to monitor the behavior of a variety of live cells. The prices of all parts required to fabricate the DFCMS are shown in Supplementary Table S1.

Performance evaluation of the monitoring system

To measure the magnification of the monitoring system, a stage micrometer was used in a bench top microscope (BX51, Olympus Co., Tokyo, Japan). The field of view (FoV) was determined by comparing two images taken by the benchtop microscope and the cell monitoring system. The resolution of the cell monitoring system was evaluated using the 1951 USAF Resolution Test Target (1951 USAF Hi-Resolution Target; R1DS1P, Thorlabs, Newton, NJ, USA). The 1951 USAF resolution test chart was imaged, and the pixel intensities across the patterns on the positive test chart were measured and plotted using

ImageJ software (NIH, Bethesda, MD, USA, http://imagej.nih.gov/ij/). The resolution of the monitoring system was determined based on the measurement results.

The dark field performance of the monitoring system was evaluated with a bench-top microscope (BX51, Olympus Co., Tokyo, Japan) and dark field images of this system. The samples used were micro polystyrene particles (Sigma–Aldrich, Oakville, ON, Canada) of (3 and 10) mm diameter and whole blood. This experimental procedure was approved by the institutional review board (IRB) of Jeonbuk National University (IRB File No. JBNU 2018-01-004-001). Whole blood was collected from healthy human donors with informed consent.

Cell monitoring

HeLa, 3T3-L1, CCD-986sk, HT-29, and MDA-MB-231 cells were supplied by the Korean cell line bank (10002, 10092.1, 21947, 30038, and 30026, KCLB, Seoul, South Korea). All cells were cultured using standard protocols.

To compare the images of fluorescence microscopy, phase contrast microscopy, and dark field microscopy, human skin fibroblast CCD-986sk cells were prepared at the cell culture slide (cat. no. 30102, SPL Co., Pocheon, Gyeonggi-do, South Korea). After the 1st, 3rd, 5th, and 7th day of culture, the medium was removed, and the cells were washed twice with 1X PBS buffer. Cells were then fixed with 2 % Paraformaldehyde and 2 % Glutaraldehyde at 37 °C for 20 min, and permeabilized with 0.1 % Triton X-100 for 10 min at room temperature (RT). The fixed and permeated cells were washed, and treated with Alexa Fluor 488-phalloidin (A12379, Invitrogen, Paisley, UK) for 30 min at RT for cell staining. After washing twice with 1X PBS, the cell staining with DAPI (P36935, Invitrogen, Paisley, UK) was completed after 5 min incubation at RT. Afterwards, fluorescence, phase contrast, and dark field images were taken by the bench top microscope, and DFCMS, respectively.

Cells of HeLa and 3T3-L1 were photographed in time-lapse. HeLa and 3T3-L1 cells were prepared in a 90 mm cell culture dish (cat. no. 20100, SPL Co., Pocheon, Gyeonggi-do, South Korea) at a density of 1.5 x 10^4 cells per plate, respectively. Thereafter, cell monitoring was performed after incubating for 12 h under a 37 °C and 5 % CO_2 condition in a cell culture incubator. Cell proliferation and death were captured at 10 min intervals, to prevent temperature rise of the medium due to the heat emitted from the camera, and to avoid the phototoxicity of the LED.

A cell culture dish coated with multi-walled carbon nanotubes (MWCNT) (CNT MR99, Carbon Nano Material Technology Co., Ltd., Pohang, Gyeongsangbuk-do, South Korea) was prepared for 3D projection image observation. 3T3-L1 cells were prepared on MWCNT-coated cell culture dishes at a density of 1.5 x 10^4 cells per plate. Cell monitoring was taken continuously every 30 min for 7 days (d).

To observe 3D projections of cells on glass beads with high hardness, HT-29 cells were prepared as glass beads at a density of 1 x 10^4 cells per plate. Glass beads (cat.no SI.5215, DAIHAN Scientific, Wonju, Gangwon-do, South Korea) of 150 μm diameter were filtered through standard test sieves Nos. 80 and

100. Thereafter, cell monitoring was performed after incubating for 12 h under a 37 °C and 5 % CO_2 condition in a cell culture incubator. Long-term cell monitoring was performed, taking an image every 30 min for 8 d.

For 3D projections of cell observation on GelMA beads with low hardness, MDA-MB-231 cells were prepared with GelMA beads at a density of 1 x 10^4 cells per plate. GelMA solution was prepared by mixing 8 wt.% of gelatin methacrylates in 1X PBS. GelMA beads was manufactured by flow focusing method by injection through a 34 gauge needle in mineral oil containing 25 wt.% Span 80 surfactant that was rotating in a cylinder. GelMA beads with a size of 150 μm were sufficiently washed. Long-term cell monitoring was captured at 30 min intervals for 10 d.

The cell monitoring system was controlled by a program using LabView 2017 (National Instruments Corp., Austin, TX, USA) to continuously capture images that were stored on a flash disk. Cell monitoring images were analyzed using ImageJ image processing software. In particular, the cell division and death processes of HeLa and 3T3-L1 cells were analyzed after conversion of single cell images into contour images using OriginPro (Originlab Corp., Northampton, MA, USA) program.

Results And Discussion

Characterization and evaluation of the cell monitoring system

One of the most important considerations in dark field imaging is the dark field filter, which plays a key role in determining the contrast of the image. Five types of dark field filters were designed and fabricated to characterize the effect of image contrast on the position of the dark field filter gap. Figure 2a shows a schematic of the experimental apparatus with 20x magnification according to the position of the inner diameter of the dark field filter with a fixed gap. Figures 2b & c indicate the characterization as a function of focal length and DFF_{ID}. The optimal dark field filter was determined by comparing the image sharpness of a plant specimen (Stem of monocotyleden, 100 Prepared microscope slides, KKmoon, Shenzhen, China). Increasing the focal length from (28 to 33) mm in the cell motoring system enhanced the contrast of the specimen image. Moving the position of the inner diameter of dark field filter from (19 to 23) mm caused a decrease in the perceived brightness of the specimen. These results showed that the incident light angle adjusted by the dark field filter could control light scattering of the dark background to enhance contrast in the specimen. To determine the highest contrast image, the image seen at focal length of 33 mm and DFF_{ID} of 21 mm was competitive with the image at focal length of 32 mm and DFF_{ID} of 21 mm. Considering both the focal length and gap position of the dark field filter, the optimal image was determined at a focal length of 32 mm and DFF_{ID} of 21 mm, because the unpicked image was needed to correct the chromatic aberration of the lens.

Figures 2d–f show that the performance of the cell monitoring system was evaluated using a benchtop microscope (Olympus BX51 microscopy). The horizontal FoV of the cell monitoring system was measured as 940 μm, and the vertical FoV of the cell monitoring system was measured as 696 μm, which

were similar values to those of the benchtop microscope. The fixed FoV of the cell monitoring system was large enough to observe cells. Two tools imaged the bright and dark field features of the polystyrene particles (Fig. 2d), whole blood (Fig. 2e), and CCD-986sk human dermal fibroblast cells (Fig. 2f). All samples had the commonality that samples that were invisible in the bright field or phase contrast images were clearly observed from sub-micron size up to custom micron size in the dark field images. This showed the availability of the dark field function of the cell monitoring system. Also, it proved that the performance of the cell monitoring system was comparable to that of the benchtop microscope in terms of long-term dark field imaging, as shown in Fig. 2f.

Comparison of the 3D projection performance of DFCMS and the bench top microscope

Figure 3 shows a comparison of the bright field and phase contrast mode of the benchtop microscope and the dark field mode of DFCMS based on the projection of 3D cells onto a 2D plane. Snapshots of the experiments were taken according to each imaging mode, with the MDA-MB-231 cells sufficiently proliferated. The 2D plane represents the bottom surface of a typical cell culture dish. In the 2D plane, MDA-MB-231 cells were observed more clearly in the phase contrast mode of the benchtop microscope, and in the dark field mode of the DFCMS, than in the bright field mode of the benchtop microscope. In DFCMS, high-contrast images were obtained, compared to the phase contrast mode of a benchtop microscope. On the CNT-coated surface, MDA-MB-231 cells were observed much more clearly in the dark field mode of DFCMS, than in the phase contrast mode of the benchtop microscope. In addition, DFCMS showed high resolution that clearly distinguished the cell membrane and nucleus, and agglomerated CNT networks were also clearly observed. To increase the diffuse reflection of incident light, the Pt-coated CNT network sample was observed to be shinier than the non-Pt-coated sample. Glass beads and GelMA beads were introduced to observe the three-dimensionally projected cells. In the bright field mode of the benchtop microscope, the shape of the MDA-MB-231 cells was observed on the bottom of the cell culture dish, similar to the image in the phase contrast mode. This is because the incident light passes through the glass beads to induce diffuse reflection, and obtains a phase contrast effect on its own, so the cells are observed clearly. In the dark field mode of DFCMS, high-contrast images were obtained of both the cells at the bottom of the cell culture dish, and the cells on the surface of glass beads. For the GelMA bead, the proliferation of cells on the surface of the GelMA bead was confirmed in bright field mode and phase contrast mode on the benchtop. In the benchtop bright field mode, the outline of the GelMA bead was not clear, whereas in the phase contrast mode, the outline of the GelMA bead was clearly observed. Conversely, in the phase contrast mode, cells on the surface of the GelMA bead were out of focus, due to excessive phase contrast effect. In the dark field mode of DFCMS, the clear outline of the GelMA bead and the cells that had proliferated on the bead surface were seen with high contrast.

Short-term and long-term cell culture monitoring

Figures 4a & b show that the dark field cell monitoring system was capable of short-term (3 d) cell culture monitoring after seeding cells. HeLa and 3T3-L1 cells were prepared for short-term monitoring as described in the methods section. The time-lapse videos of the short-term live cell imaging experiments

can be found in the Supplementary Video S1. The videos reveal that fully automated time-resolved dark field imaging served by the cell monitoring system could visualize how cells were constantly changing morphologically in detail. Also, Figs. 4c & d show that dark field imaging was able to quantitatively measure the cell confluency rate as a function of time. As a result of fundamental analysis based on the dark field imaging, we could directly confirm that the confluency rate of HeLa cells was twice as fast as that of 3T3-L1 cells. The acquiring of such *in situ* analysis would be of advantage for high-throughput real-time cell monitoring.

Monitoring of cell division and death

Single cell monitoring for *in situ* understanding of the cell division and death processes was performed in a label-free and non-destructive manner. Figure 5a shows the division of a single HeLa cell in terms of morphology. The process monitoring was repeated three times. During the division process of about 70 min, each image to represent an important event was clearly taken. In the beginning, HeLa cell was in the form of a mononucleated giant cell at resting stage. Then, gradual change to round shape was found, showing distinct membrane. After 40 min, the parent cell was ready to divide into two daughter cells. Its membrane seemed to be thicker. However, after cell separation, the membranes looked faint, owing to spreading out. As the cell division process was completed, the two daughter cells began to change into mononucleated giant cells. It is noteworthy here that during cell division, the live migration of cell lipids could be observed. Although lipid drops smaller than the submicron beyond the resolution limit of the monitoring system appeared clustered rather than individual drops, analysis of color contour based on lipid offered *in situ* information for the lipid accumulation induction of HeLa cell to the stage before cell division. Figure 5b shows that the division of a single 3T3-L1 cell was monitored to confirm the monitoring performance of the system using a different cell type. Unlike the HeLa cell, the 3T3-L1 cell initially showed the large appearance of a single nucleus at resting stage. Then after 30 min, lipids were gathered in more concentrated manner, than those of the HeLa cell, which made the cell smaller than the HeLa cell. This lipid focusing feature allowed lipid migration to be clearly seen, resulting in clearer imaging of the events of cell division. This approach can offer the unique advantage of continuous cell monitoring in the process of cell division.

Another important use of the cell monitoring system is the real-time monitoring of cell death. Figure 5c shows the cell morphology observed for 1,290 min of the cell death of HeLa cells. Cell death proceeded by shutting off the CO_2 gas in the cell incubator. After 480 min, the HeLa cells showed shrinkage of the cell membrane, which had been blurred. After 720 min, HeLa cells were transformed into a circular shape. After 1,270 min, the shape of the HeLa cells was close to a perfect circle, and showed a sharp, high-contrast morphology. After an additional 20 min of observation, the HeLa cells showed no further morphological changes. In the early stage of cell death in Fig. 5d, 3T3-L1 cell death showed cell membrane contraction (~900 min) similar to that of HeLa cells. However, after 900 min, 3T3-L1 cell death changed the cell morphology to a circular shape within a faster time (960 – 1,020) min than HeLa cell death. Additionally, although the cells were observed for sufficient duration, the circular morphology did not change to a different shape.

Long-term monitoring of DFCMS for the projection of 3D geometry

Figure 6 shows long-term monitoring of different cells in a three-dimensional structure projected onto a two-dimensional plane. Each cell monitoring was performed for 10 days, and related videos can be found in Supplementary Video S2. Figure 6a shows the results of long-term monitoring of 3T3-L1 cells on an aggregated three-dimensional CNT network. In the monitoring image, the black color represents CNT, while the gray color represents the cell culture dish surface. The thickness of the CNT layer is about 50 μm. The figure shows that in DFCMS, 3T3-L1 cells were observed with distinct and high contrast. Because the thickness of the CNT layer is thin, 3T3-L1 cells showed cell migration, regardless of the surface of the CNT and the cell culture dish. As a result, the proliferation of 3T3-L1 cells increased steadily from d (1 to 10) (Fig. 6b). Figure 6c shows the long-term monitoring of HT29 cells on a glass bead. In DFCMS, the outline of the glass bead is very clearly expressed. Due to the clean incident light, some of the glass bead surfaces are DFF projected. The diameter of the glass bead is about 150 μm, which is about (11 to 13) times larger than typical HT29 cells. The focus of the DFCMS was on the edge of the glass bead. Cell monitoring was commenced after the HT29 cells were completely submerged under the glass bead. The proliferation of HT29 cells did not show any significant change from d (1 to 3). However, after 4 d, the bottom of the cell culture dish was saturated with HT29 cells, and some of the cells came up along the surface of the glass bead. On d 6, HT29 cells sufficiently proliferated on the glass bead were projected by the incident light onto the bottom of the cell culture dish. On d 10, HT29 cells were observed on the glass bead and the bottom of the cell culture dish, regardless of focus. The proliferation of HT29 cells on the glass bead showed a trend of increasing exponentially from d 4, when the bottom of the cell culture dish was saturated (Fig. 6d).

Figure 6e shows the proliferation behavior of MDA-MB-231 cells on GelMA beads. The diameter of the GelMA beads was made about 150 μm, which is (6–8) times the size of a typical MDA-MB-231 cell. As with the glass bead, we fixed the focus on the edge of the GelMA bead, and started monitoring. Overall, MDA-MB-231 cell proliferation proceeded more rapidly than did HT29 cell proliferation. After 5 days, MDA-MB-231 cells that had proliferated sufficiently on the bottom of the cell culture dish began to proliferate on the surface of the GelMA bead. Cells that proliferated on GelMA beads were observed with sharp and high contrast by the incident light. MDA-MB-231 cells adapted to GelMA beads proliferated much faster than HT29 cells on glass beads. Saturated cell proliferation on the GelMA bead descended back to the bottom, and was stacked in multiple layers from the 3D projected GelMA bead. Figure 6f shows that MDA-MB-231 cells on GelMA bead proliferated nearly twice as steeply as HT29 cells on glass beads.

Conclusions

We introduced a new dark field-based portable monitoring system with high contrast by transmitting optimal incident light into the specimen. The miniaturized, low-cost (less than $360) cell monitoring system consisted of LED light, dark field filter, condenser lens, and CMOS sensor with reversed camera lens. The dark field filter was designed, fabricated, and tested to optimize the incident light angle that

could suppress light scattering of the dark background, leading to enhanced contrast in specimens. Its contrast-enhanced high-resolution could make definite *in situ* monitoring functions of cell density and viability possible for short-term and long-term monitoring. Single cell monitoring for rapid understanding of the cell division and death processes was successfully performed in a label-free and non-destructive manner. Also, the lipid focusing feature allowed lipid migration to be clearly seen, resulting in clearer imaging of the events of cell division and death. Acquiring such an *in situ* high-contrast monitoring by optimal dark field illumination would provide a powerful approach for high-throughput real time cell monitoring in the field of biomedical engineering.

Declarations

Acknowledgements

This work was supported by the National Research Foundation (NRF) of Korea, funded by the Ministry of Science and ICT (grant numbers: NRF-2020R1A4A2002817 and 2019R1I1A3A01060695). This paper was supported by research funds of Jeonbuk National University in 2020. This research was supported by "Research Base Construction Fund Support Program" funded by Jeonbuk National University in 2018.

Author contributions

Y. J.: Conceptualization, Methodology, Investigation, Data Curation, Formal Analysis, Visualization, Writing-Original Draft; **S. H.:** Methodology, Data Curation, Investigation, Visualization, Writing-Original Draft; **C. S.:** Supervision, Writing-Review and Editing; **J. J.:** Supervision, Writing-Review and Editing; **J. O.:** Supervision, Funding Acquisition, Writing-Review and Editing

Competing interests: The authors declare no competing financial interest.

References

1 Descloux, A. *et al.* Combined multi-plane phase retrieval and super-resolution optical fluctuation imaging for 4D cell microscopy. *Nat. Photonics* **12**, 165-172, doi:10.1038/s41566-018-0109-4 (2018).

2 Pérez Cota, F. *et al.* High resolution 3D imaging of living cells with sub-optical wavelength phonons. *Sci. Rep.* **6**, 1-11, doi:10.1038/srep39326 (2016).

3 Taute, K., Gude, S., Tans, S. & Shimizu, T. High-throughput 3D tracking of bacteria on a standard phase contrast microscope. *Nat. Commun.* **6**, 1-9, doi:10.1038/ncomms9776 (2015).

4 Liu, H. *et al.* A liquid thermal gradient refractive index lens and using it to trap single living cell in flowing environments. *Lab Chip* **17**, 1280-1286, doi:10.1039/C7LC00078B (2017).

5 Habaza, M. *et al.* Rapid 3D refractive-index imaging of live cells in suspension without labeling using dielectrophoretic cell rotation. *Adv. Sci.* **4**, 1600205, doi:10.1002/advs.201600205 (2017).

6 Gundlach, H. Phase contrast and differential interference contrast instrumentation and applications in cell, developmental, and marine biology. *Opt. Eng.* **32**, 3223-3228, doi:10.1117/12.142945 (1993).

7 Bereiter Hahn, J., Fox, C. H. & Thorell, B. Quantitative reflection contrast microscopy of living cells. *J. Cell Biol.* **82**, 767-779, doi:10.1083/jcb.82.3.767 (1979).

8 Chang, T., Shin, S., Lee, M. & Park, Y. Computational approach to dark-field optical diffraction tomography. *APL Photonics* **5**, 040804, doi:10.1063/1.5130529 (2020).

9 Lee, C. *et al.* Label-free three-dimensional observations and quantitative characterisation of on-chip vasculogenesis using optical diffraction tomography. *Lab Chip* **21**, 494-501, doi:10.1039/d0lc01061h (2021).

10 Shin, S., Kim, D., Kim, K. & Park, Y. Super-resolution three-dimensional fluorescence and optical diffraction tomography of live cells using structured illumination generated by a digital micromirror device. *Sci. Rep.* **8**, 1-8, doi:10.1038/s41598-018-27399-w (2018).

11 Kim, K. *et al.* Optical diffraction tomography techniques for the study of cell pathophysiology. *J. Biomed. Photonics Eng.* **2**, 020201, doi:10.18287/jbpe16.02.020201 (2016).

12 Scholler, J. *et al.* Dynamic full-field optical coherence tomography: 3D live-imaging of retinal organoids. *Light Sci. Appl.* **9**, 1-9, doi:10.1038/s41377-020-00375-8 (2020).

13 Kozacki, T., Kujawińska, M. & Kniażewski, P. Investigation of limitations of optical diffraction tomography. *Opto-electron. Rev.* **15**, 102-109, doi:10.2478/s11772-007-0006-8 (2007).

14 Parikesit, G. O., Darmawan, M. & Faisal, A. Quantitative low-cost webcam-based microscopy. *Opt. Eng.* **49**, 113205, doi:10.1117/1.3517747 (2010).

15 Greenbaum, A. *et al.* Imaging without lenses: achievements and remaining challenges of wide-field on-chip microscopy. *Nat. Methods* **9**, 889-895, doi:10.1038/nmeth.2114 (2012).

16 Greenbaum, A., Akbari, N., Feizi, A., Luo, W. & Ozcan, A. Field-portable pixel super-resolution colour microscope. *PLoS One* **8**, e76475, doi:10.1371/journal.pone.0076475 (2013).

17 Navruz, I. *et al.* Smart-phone based computational microscopy using multi-frame contact imaging on a fiber-optic array. *Lab Chip* **13**, 4015-4023, doi:10.1039/c3lc50589h (2013).

18 Sanz, M., Picazo Bueno, J. Á., Granero, L., García, J. & Micó, V. Compact, cost-effective and field-portable microscope prototype based on MISHELF microscopy. *Sci. Rep.* **7**, 43291, doi:10.1038/srep43291 (2017).

19 Purwar, P. *et al.* High-resolution cost-effective compact portable inverted light microscope. *J. Microsc.* **273**, 199-209, doi:10.1111/jmi.12775 (2019).

20 Jiang, S. *et al.* Wide-field, high-resolution lensless on-chip microscopy via near-field blind ptychographic modulation. *Lab Chip* **20**, 1058-1065, doi:10.1039/c9lc01027k (2020).

21 Sund, S. E., Swanson, J. A. & Axelrod, D. Cell membrane orientation visualized by polarized total internal reflection fluorescence. *Biophys. J.* **77**, 2266-2283, doi:10.1016/s0006-3495(99)77066-9 (1999).

22 Wei, N., You, J., Friehs, K., Flaschel, E. & Nattkemper, T. W. In situ dark field microscopy for on-line monitoring of yeast cultures. *Biotechnol. Lett.* **29**, 373-378, doi:10.1007/s10529-006-9245-x (2007).

23 Taylor, M. A. & Bowen, W. P. Enhanced sensitivity in dark-field microscopy by optimizing the illumination angle. *Appl. Opt.* **52**, 5718-5723, doi:10.1364/ao.52.005718 (2013).

24 Cybulski, J. S., Clements, J. & Prakash, M. Foldscope: origami-based paper microscope. *PLoS One* **9**, e98781, doi:10.1371/journal.pone.0098781 (2014).

25 Walzik, M. P. *et al.* A portable low-cost long-term live-cell imaging platform for biomedical research and education. *Biosens. Bioelectron.* **64**, 639-649, doi:10.1016/j.bios.2014.09.061 (2015).

26 Sharkey, J. P., Foo, D. C., Kabla, A., Baumberg, J. J. & Bowman, R. W. A one-piece 3D printed flexure translation stage for open-source microscopy. *Rev. Sci. Instrum.* **87**, 025104, doi:10.1063/1.4941068 (2016).

27 Jung, D. *et al.* Smartphone-based multi-contrast microscope using color-multiplexed illumination. *Sci. Rep.* **7**, 7564, doi:10.1038/s41598-017-07703-w (2017).

28 Sun, D. & Hu, T. Y. A low cost mobile phone dark-field microscope for nanoparticle-based quantitative studies. *Biosens. Bioelectron.* **99**, 513-518, doi:10.1016/j.bios.2017.08.025 (2018).

29 Huang, Y. C., Lei, K. F., Liaw, J. W. & Tsai, S. W. The influence of laser intensity activated plasmonic gold nanoparticle-generated photothermal effects on cellular morphology and viability: a real-time, long-term tracking and monitoring system. *Photochem. Photobiol. Sci.* **18**, 1419-1429, doi:10.1039/c9pp00054b (2019).

30 Guo, Y. *et al.* Activated plasmonic nanoaggregates for dark-field situ imaging for HER2 protein imaging on cells surface. *Bioconjug. Chem.* **31**, 631-638, doi:10.1021/acs.bioconjchem.9b00787 (2020).

Figures

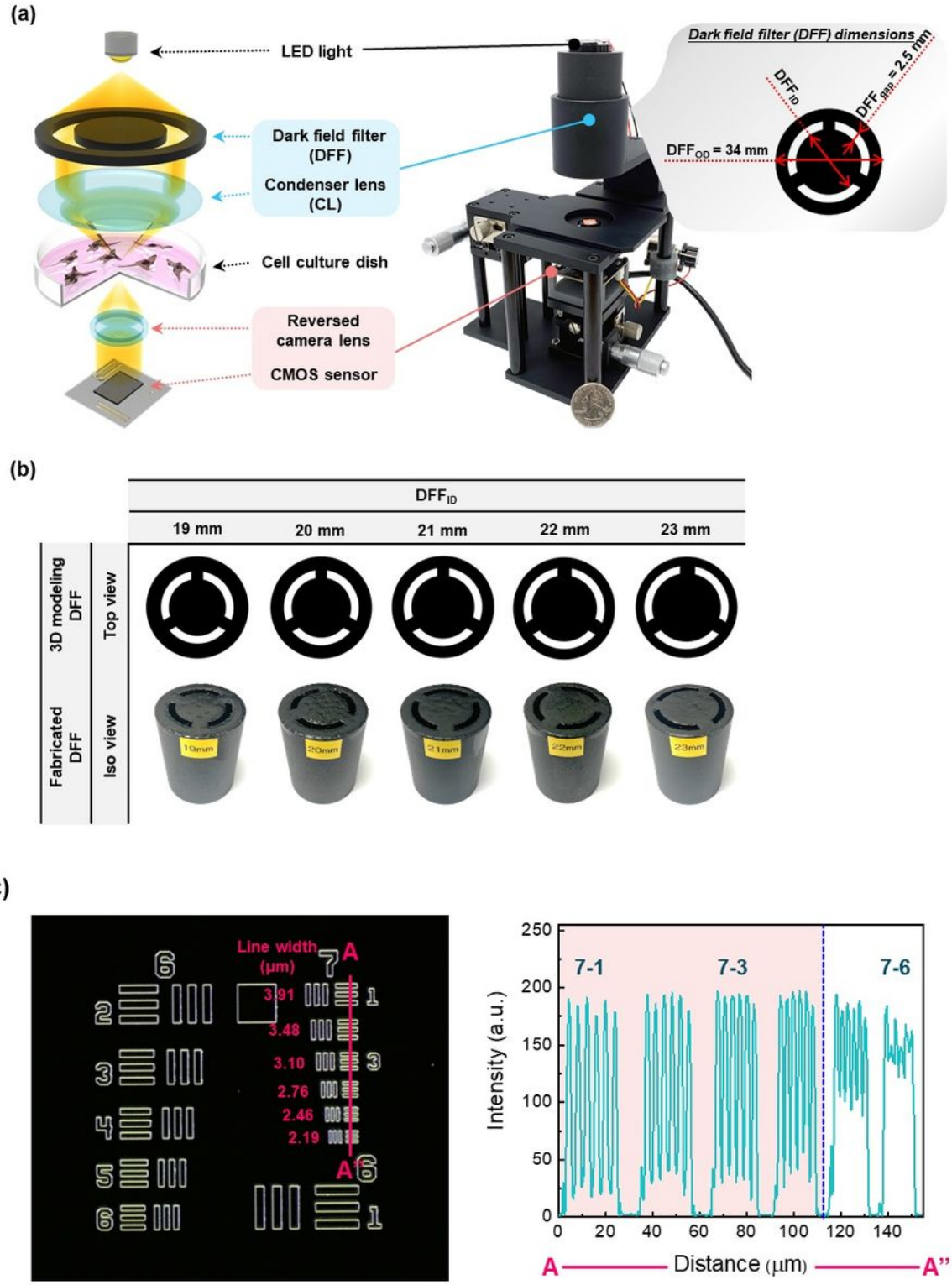

Figure 1

(a) Schematic of the DFCMS. (b) Top view of the 3D modeled DFF and iso view of the 3D printed DFF. (c) Resolution evaluation of DFCMS using a 1951 USAF resolution test target.

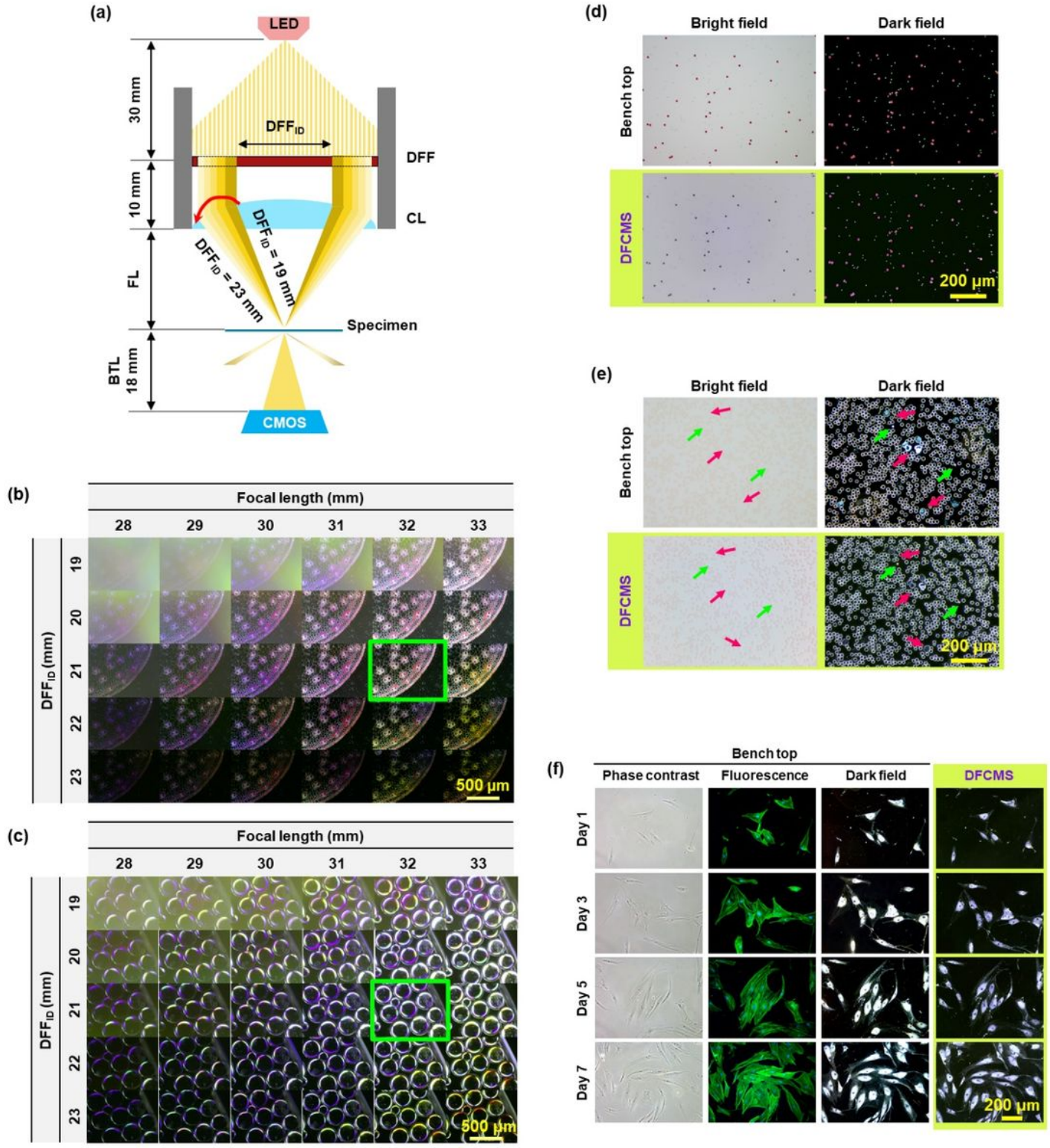

Figure 2

(a) Structure of DFCMS including dark field filter and light path in dark field mode. (b) Evaluation of chromatic aberration using 2D plant samples for focal length and inner diameter of DFF. (c) Evaluation of chromatic aberration using 3D glass beads for focal length and inner diameter of DFF. (d) Comparison of benchtop microscope and DFCMS using polystyrene beads (red bead: 10 μm, blue bead: 3 μm); (e) Comparison of benchtop microscopy and DFCMS using whole blood (red blood cells, white blood cells,

platelets); (f) Comparison of phase contrast, fluorescence, and dark field mode of benchtop microscope and dark field mode of DFCMS using CCD-986sk cells.

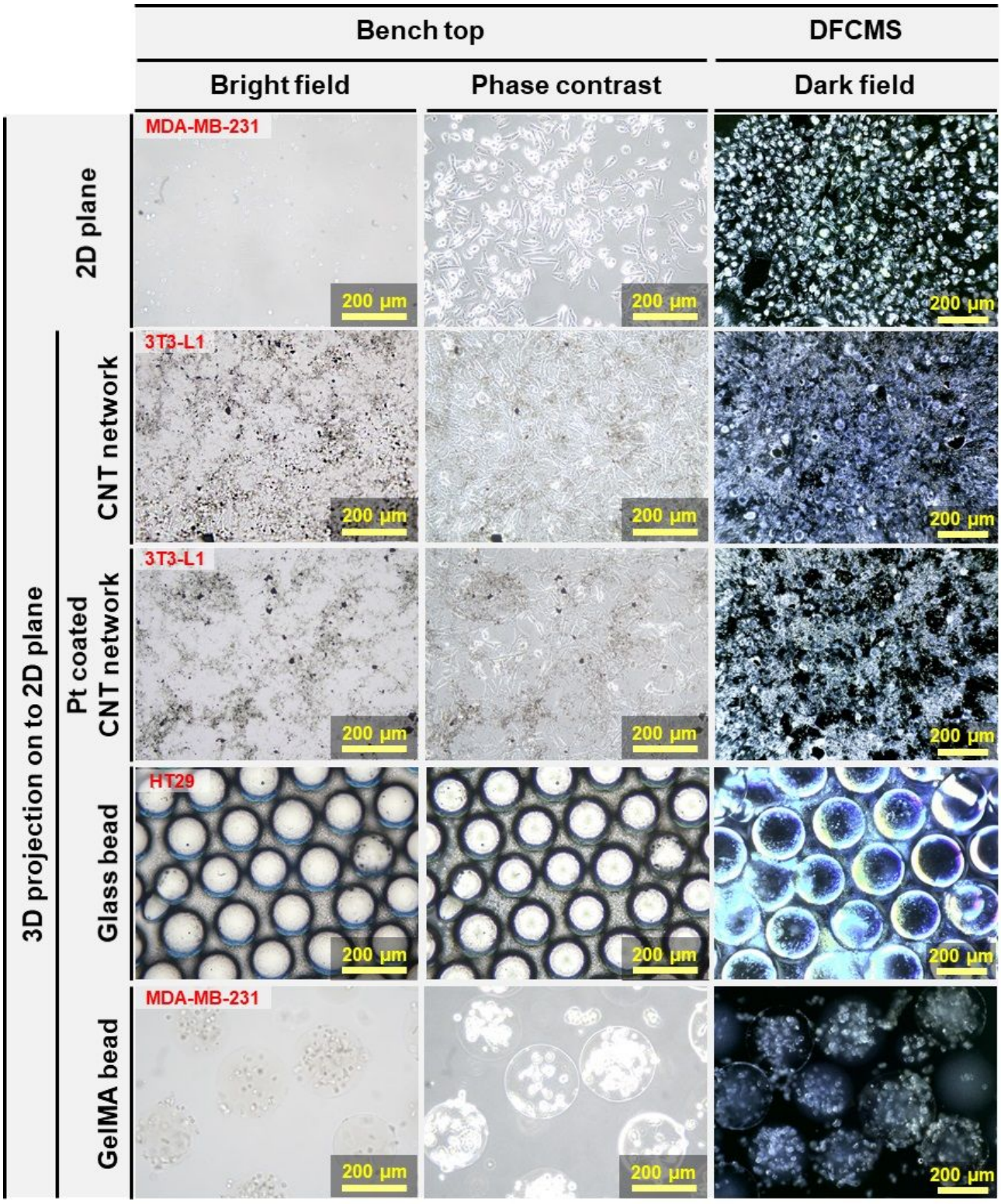

Figure 3

Comparison of 3D projections of benchtop microscopy and DFCMS with cell proliferation (CNT network, Pt coated CNT network, Glass bead, and GelMA bead).

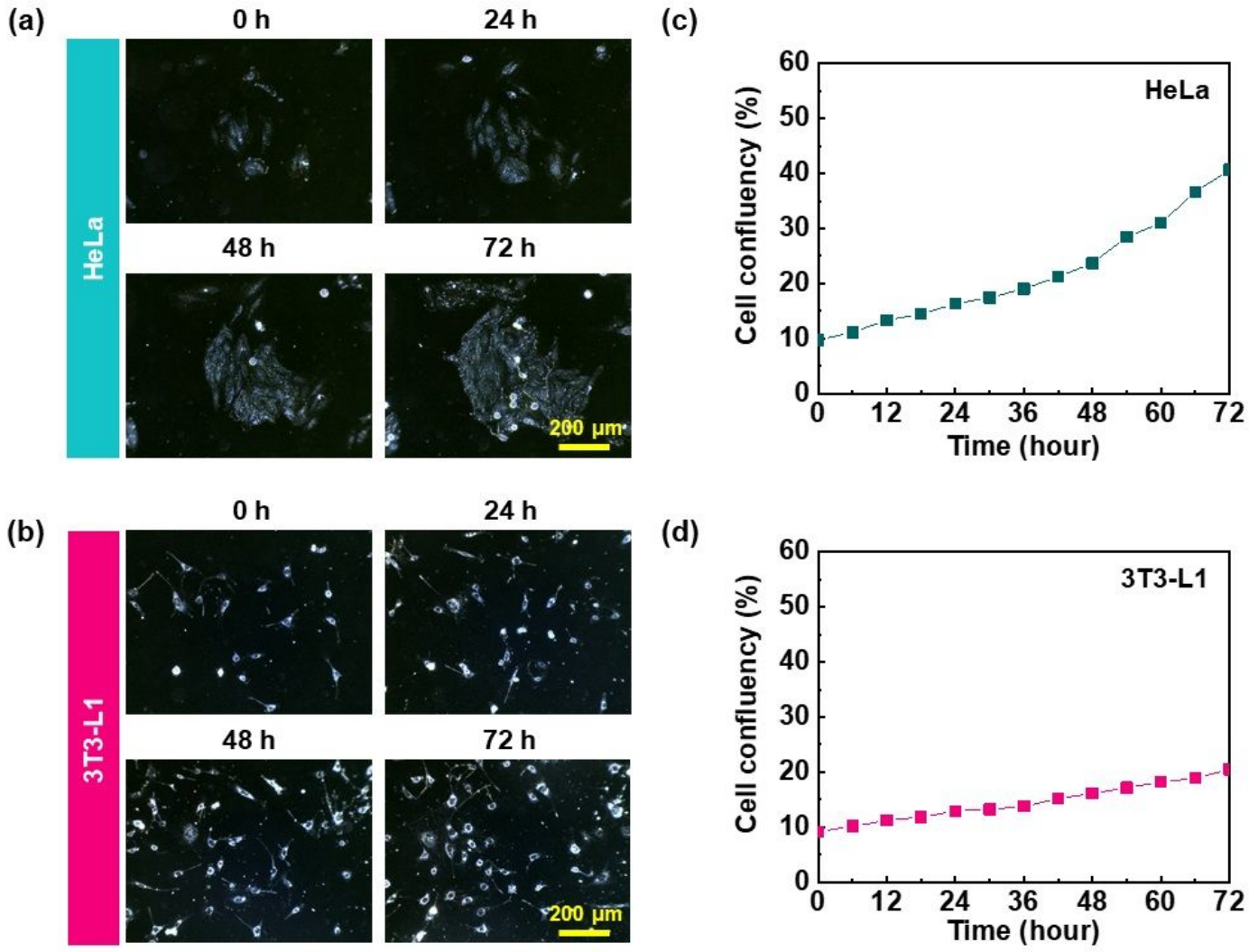

Figure 4

Cell proliferation images at (0, 24, 48, and 72) h after cell seeding. (a) HeLa, and (b) 3T3-L1 cells; Cell confluency plot of (c) HeLa, and (d) 3T3-L1 cells.

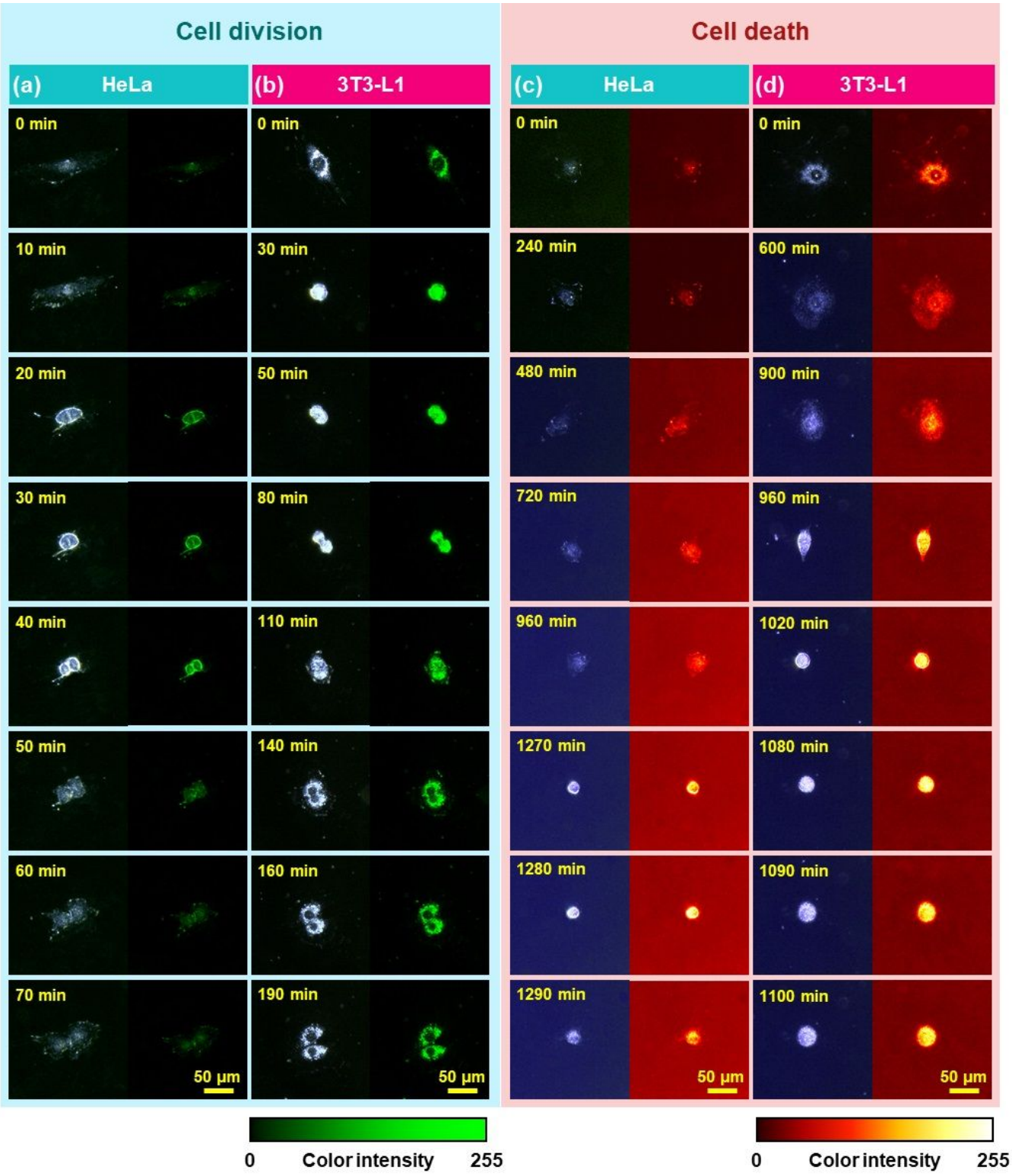

Figure 5

Contour image of the cell division process. (a) HeLa, and (b) 3T3-L1 cells; contour image of cell death process of (c) HeLa, and (d) 3T3-L1 cells.

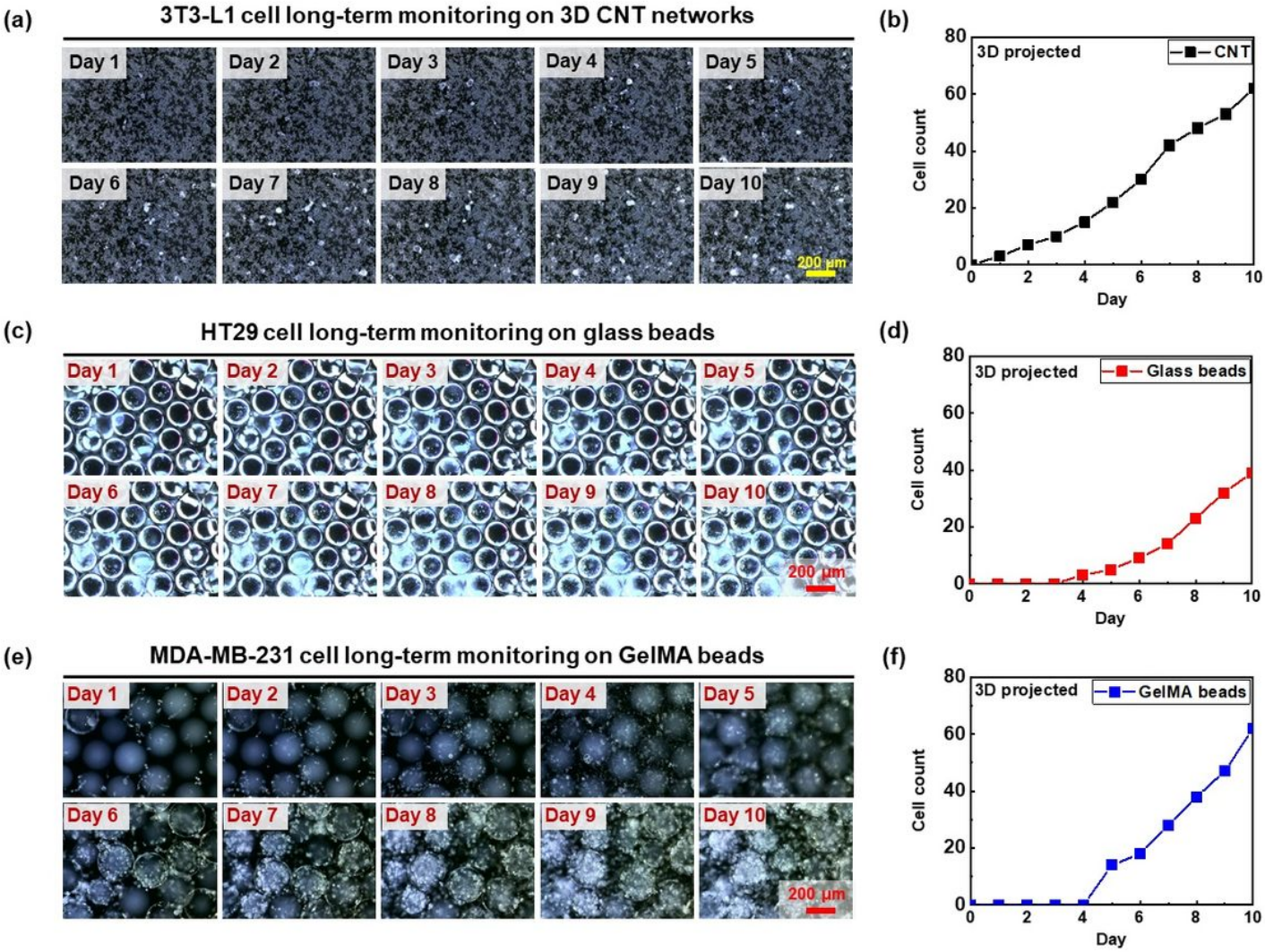

Figure 6

Long-term monitoring of DFCMS for the projection of 3D geometry. (a) Monitoring of 3T3-L1 cells on a 3D CNT network, and (b) Cell count plot over time of 3T3-L1 cells. (c) Monitoring of HT29 cells on glass beads, and (d) Cell count plot over time of HT29 cells. (e) Monitoring of MDA-MB-231 cells on GelMA beads, and (f) Cell count plot over time of MDA-MB-231 cells.

Supplementary Files

This is a list of supplementary files associated with this preprint. Click to download.

- SupplementaryInformation.docx
- VideoS2.mp4
- VideoS1.mp4